Nanosphere Templated Continuous PEDOT:PSS Films with Low Percolation Threshold for Application in Efficient Polymer Solar Cells

ARTICLE *in* ACS NANO · AUGUST 2012

Impact Factor: 12.88 · DOI: 10.1021/nn3022926 · Source: PubMed

4 AUTHORS, INCLUDING:

Dong Jin Kang

Korea Advanced Institute of Science and Tec…

30 PUBLICATIONS **356** CITATIONS

SEE PROFILE

Nanosphere Templated Continuous PEDOT:PSS Films with Low Percolation Threshold for Application in Efficient Polymer Solar Cells

Dong Jin Kang,[†] Hyunbum Kang,[†] Ki-Hyun Kim,[†] and Bumjoon J. Kim[†,*]

[†]Department of Chemical and Biomolecular Engineering, Korea Advanced Institute of Science and Technology (KAIST), Daejeon 305-701, Republic of Korea

ABSTRACT Nanometer-sized monodisperse polystyrene nanospheres (PS NS) were designed as an opal template for the formation of three-dimensionally continuous poly(3,4-ethylenedioxythiophene):poly(styrene sulfonate) (PEDOT:PSS) films. The resultant films were successfully applied as the anode buffer layer (ABL) to produce highly efficient polymer solar cells (PSCs) with enhanced stability. The conductivity of the PS NS-PEDOT:PSS films was maintained up to $\phi_{PS} = 0.75-0.80$, indicating that the formation of continuous PEDOT:PSS films using PS NS templates was successful. To demonstrate the applicability of the PS NS-PEDOT:PSS film for organic electronics, the PS NS-PEDOT:PSS films were used as ABLs in two different PSCs: P3HT:PCBM and P3HT:OXCBA. The photovoltaic performances of both PSCs were maintained up to $\phi_{PS} = 0.8$. In particular, the power conversion efficiency of the P3HT:OXCBA PSC with a PS NS-PEDOT:PSS ABL ($\phi_{PS} = 0.8$) was greater than 5% and the air stability of the device was significantly enhanced.

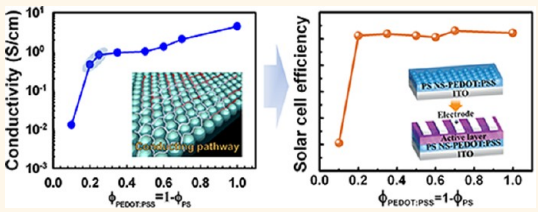

KEYWORDS: nanosphere · PEDOT:PSS · opal template · polymer solar cell · air stability

Conducting polymers have attracted a great deal of attention due to their potential use in many future applications in low cost, flexible, and printable electronic devices.[1−9] In particular, poly(3,4-ethylenedioxythiophene):poly(styrene sulfonate) (PEDOT:PSS) has been used commercially in solid electrolyte capacitors, antistatic coatings, and other applications.[10,11] In addition, PEDOT:PSS polymers are the most commonly used anode buffer layers (ABLs) in solution-processed organic electronics (*e.g.*, polymer solar cells (PSCs) and organic light-emitting diodes (OLED) due to their high electrical conductivity and water solubility.[10,12−14] However, the acidity and hygroscopic nature of PEDOT:PSS can lead to serious degradation of organic electronics.[15,16] For example, the PEDOT:PSS can etch the ITO film and cause interface instability *via* indium diffusion into the active layer.[17,18] In addition, the relatively high cost and poor mechanical properties of PEDOT:PSS-based ABLs could limit the commercialization of the organic electronics.[19,20]

To achieve high conductivity, stability, and low cost, blending the conducting polymer with a low-cost polymer matrix that can provide the desired mechanical properties without interfering with the electrical properties of the conducting polymer is a promising solution.[21−25] The blending approach requires the conducting polymer phase to be continuous, the percolation threshold to be low, and the length scale to be controlled.[26] For instance, simple blending usually does not allow the degree of morphological control that ensures a continuous conducting polymer because polymer blends tend to be macrophase separated.[27,28] The opal template approach, which is based on self-assembled colloids with a uniform size distribution, is a powerful method of producing continuous conducting polymer films from small amounts of conducting polymers without damaging the electrical properties.[29−33] For example, Kramer *et al.* reported a high internal polymeric phase emulsion system of a doped conducting polyaniline-phenolsulfonate polymer driven by self-assembled micrometer-sized polystyrene (PS) colloids in the presence of a block copolymer. Compared to traditional blending procedures, this process reduces the percolation threshold for electrical conductivity by a factor of 10 and increases the conductivity by several orders of magnitude.[29] As another example, Caruso *et al.* reported the preparation of an inverse opal-structured polyaniline and polypyrrole using the self-assembled structure of

* Address correspondence to bumjoonkim@kaist.ac.kr.

Received for review May 23, 2012 and accepted August 11, 2012.

Published online August 11, 2012
10.1021/nn3022926

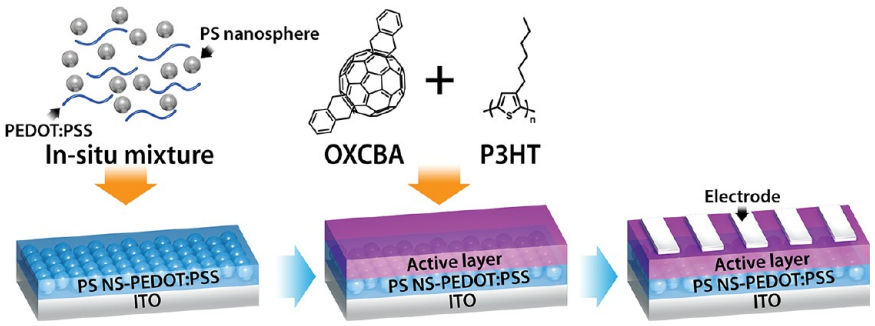

Scheme 1. Schematic illustration of the nanosphere template approach used to produce a three-dimensionally continuous conducting PEDOT:PSS film. The use of the film as an ABL resulted in highly efficient PSCs with enhanced air stability.

PS colloidal particles.[34,35] We recently reported a method for producing continuous conducting poly(triphenylamine) films with low percolation thresholds using a PS colloidal template and a gold nanoparticle compatibilizer.[31] However, to the best of our knowledge, none of the previous work that used the colloid template method focused on thin film (*i.e.*, less than 100 nm) applications. In contrast, many of the electronic and/or optical applications require the use of thin films that are less than 100 nm in thickness. In particular, while conducting PEDOT:PSS polymers are the most commonly used ABLs in solution-processed organic electronics and flexible devices, the optimal thickness of the ABL is typically less than 100 nm.[36]

In the present study, we develop a facile method for creating nanosphere-templated continuous PEDOT:PSS films and demonstrate their use as efficient and stable ABLs in PSCs (Scheme 1). First, monodisperse, 60-nm sized PS nanospheres (PS NSs) were designed and synthesized by emulsion polymerization in water. The highly stable and dispersible properties of PS NSs in water enable the PS NSs to be easily blended with PEDOT:PSS. Therefore, continuous PEDOT:PSS films were fabricated using PS NS as opal templates. To investigate the effects of the PS NS on the electrical properties of the PS NS-templated PEDOT:PSS films (PS NS-PEDOT:PSS), the conductivity and morphological behavior of the PS NS-PEDOT:PSS films were carefully measured as a function of the PS NS volume fraction (ϕ_{PS}). Surprisingly, the conductivity of PS NS-PEDOT:PSS films and the continuity of the PEDOT:PSS phase were maintained up to ϕ_{PS} = 0.75−0.80. To further demonstrate the applicability of the PS NS-PEDOT:PSS film for organic electronics, the PS NS-PEDOT:PSS film was used as an ABL in two different PSCs of poly(3-hexylthiophene):phenyl-C_{61}-butyric acid methyl ester (P3HT:PCBM) and poly(3-hexylthiophene):*o*-xylenyl C_{60} bisadduct (P3HT:OXCBA). The photovoltaic properties of both PSCs were maintained up to ϕ_{PS} = 0.8. In particular, the P3HT:OXCBA device with a PS NS-PEDOT:PSS ABL (ϕ_{PS} = 0.8) exhibited a power conversion efficiency (PCE) of greater than 5%, and the air stability of the device increased by a factor of 3.

RESULTS AND DISCUSSION

To create a continuous conducting PEDOT:PSS phase at a low concentration in the film, PS NSs were added to an aqueous solution of PEDOT:PSS. There are two important requirements for the use of PS NS as a template in thin PEDOT:PSS films, which are the following: (1) PS NSs should be well dispersed and stabilized in the same solvent (*i.e.*, water) as the PEDOT:PSS polymers and (2) the PS NSs should possess a diameter less than 100 nm with a very narrow size distribution because the optimal thickness of a PEDOT:PSS ABL for PSCs and OLEDs is typically reported to be between 50 and 70 nm.[36] To meet these requirements, monodisperse PS NSs were carefully designed and synthesized *via* emulsion polymerization in water, and the reaction conditions (*e.g.*, stabilizer concentration) were controlled. A washing procedure (*i.e.*, several cycles of centrifugation in deionized water) was used to purify the synthesized PS NSs, which resulted in 60-nm diameter PS NSs with excellent monodispersity, as shown in Figure 1a.

The morphological behavior of the PS NS-PEDOT:PSS blends was investigated as a function of the ϕ_{PS} of the PS NS-PEDOT:PSS films. First, various amounts of monodisperse PS NSs were added to an aqueous solution of PEDOT:PSS to produce different ϕ_{PS} values. The concentrations of the polymer mixtures (PS NS + PEDOT:PSS) in the water were controlled to produce PS NS-PEDOT:PSS films with similar thickness of approximately 60 nm for all different ϕ_{PS} values after spin coating the solution of the blends for 40 s at 2000 rpm onto ITO substrates. The films were thermally annealed at 150 °C for 20 min to remove water. Figure 1 shows SEM images of PS NS-PEDOT:PSS films with different ϕ_{PS} values: (a) PS NSs, (b) pristine PEDOT:PSS (ϕ_{PS} = 0), (c) PS NS-PEDOT:PSS (ϕ_{PS} = 0.3), (d) PS NS-PEDOT:PSS (ϕ_{PS} = 0.65), and (e) PS NS-PEDOT:PSS (ϕ_{PS} = 0.8). Whereas the image of the pristine PEDOT:PSS film in Figure 1b shows a homogeneous film with no contrast, SEM images of PS NS-PEDOT:PSS films in Figure 1 c and d clearly show the presence of PS NSs without macrophase separation or aggregation of the PS NSs on the micrometer scale. Additionally, as the ϕ_{PS} increased, the area occupied by the monolayered PS NS assembly

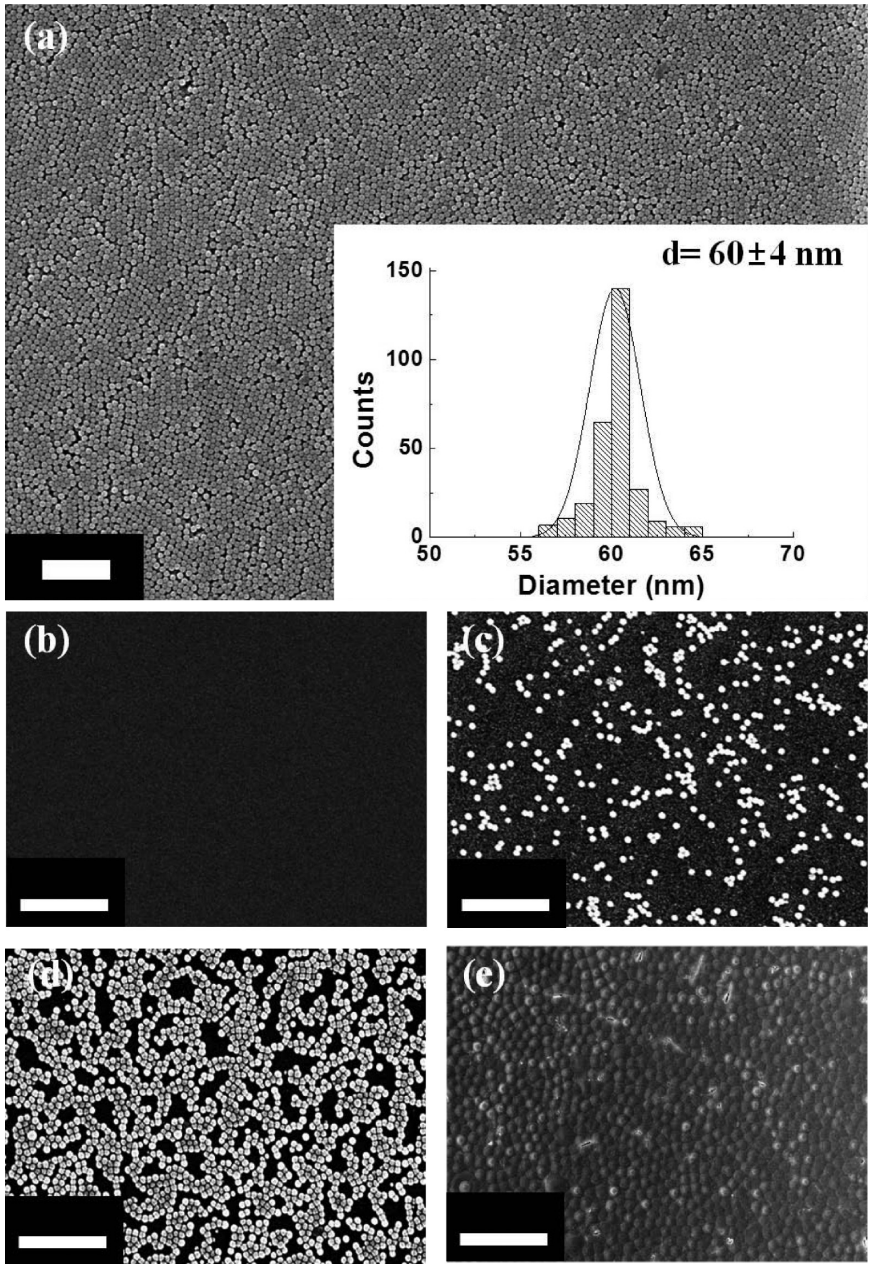

Figure 1. Surface morphologies of PS NS-PEDOT:PSS films with different ϕ_{PS} values, which were measured by SEM; (a) PS NSs and the corresponding histogram (inset) of the size distribution, (b) pristine PEDOT:PSS, (c) PS NS-PEDOT:PSS (ϕ_{PS} = 0.3), (d) PS NS-PEDOT:PSS (ϕ_{PS} = 0.65), and (e) PS NS-PEDOT:PSS (ϕ_{PS} = 0.8). The scale bar represents 1 μm in length.

in the blended film increased. As illustrated in Figure 1e, at ϕ_{PS} values greater than 0.8, the film was completely covered by a monolayer of self-assembled PS NSs. In contrast with the films in Figure 1a, void space was not observed between the PS NSs in Figure 1e, indicating that the PEDOT:PSS phase infiltrated the space surrounding the PS NSs.

To provide further evidence that the PEDOT:PSS polymer infiltrated between the PS NSs and formed a three-dimensionally continuous PEDOT:PSS phase in the PS NS-PEDOT:PSS films, the electrical conductivitiy of PS NS-PEDOT:PSS films with various ϕ_{PS} values were measured on patterned ITO/glass substrates. Figure 2 shows the conductivities of PS NS-PEDOT:PSS films with various ϕ_{PS} values. All of the conductivity values were obtained from 60-nm thick films with an area of 11 $\times$ 2 mm^2, which were prepared under identical conditions to the samples used in the morphological studies shown in Figure 1. As a control, the hole conductivity of a pure PEDOT:PSS film (*i.e.*, without PS NSs) was measured. The hole conductivity was 4.39 S/cm, which is in good agreement with the previously reported value of pristine PEDOT:PSS.[10,37] At a high ϕ_{PS} of 0.9, the conductivity was very low ($\sim 10^{-2}$ S/cm). As the ϕ_{PS} decreased and the PEDOT:PSS volume fraction ($\phi_{PEDOT:PSS} = 1 - \phi_{PS}$) increased, the conductivity of the

blend increased sharply until the $\phi_{PEDOT:PSS}$ values reached 0.2−0.25, which indicated that the $\phi_{PEDOT:PSS}$ threshold for the percolation of PEDOT:PSS (0.2−0.25) resulted in a continuous phase. The observed trend in the conductivity of the blended films was consistent with the morphological behavior, which indicated that PEDOT:PSS infiltrated into the empty spaces between the densely packed PS NSs and created a continuous phase that formed an electrical pathway. According to sphere-packing theory, the maximum volume fraction for packing monodisperse spheres into a hexagonally close-packed or face-centered cubic lattice is 0.74.[38] Therefore, if the PS NSs form a close-packed structure and function as a template, the remaining void volume fraction of 0.26 should be filled by PEDOT:PSS to form a continuous PEDOT:PSS phase between the PS NS template. Evidence of the close-packed structure of PS NSs can be clearly observed in the SEM image shown in Figure 1e. In addition, the electrical conductivity of the PS NS-PEDOT:PSS films increased dramatically until $\phi_{PEDOT:PSS}$ = 0.20−0.25. Therefore, the experimental value of $\phi_{PEDOT:PSS}$ obtained for the continuity of PEDOT:PSS phase matched the predicted theoretical value of $\phi_{PEDOT:PSS}$ = 0.26, which is the minimum value of $\phi_{PEDOT:PSS}$ that can maintain a three-dimensional, continuous minor phase within the monodispersed spheres. Although our measured percolation threshold showed reasonably good agreement with the predicted theoretical value, we would like to discuss the reason for the measured value ($\phi_{PEDOT:PSS}$ = 0.20−0.25) being slightly lower than the predicted value ($\phi_{PEDOT:PSS}$ = 0.26). First, it could be explained by the presence of protruded PS NSs in the PS NS-PEDOT:PSS ABL because of the slight mismatch between the thickness of the ABL film and the size of the PS NSs (Supporting Information, Figure S1). More importantly, the morphology of the system can reorganize upon thermal annealing at the temperature of 150 °C that was used in the fabrication of the device. In this case, the PS NSs can undergo some rearrangement upon annealing, deforming to polyhedrons wetted by the PEDOT:PSS phase, and leading to a lower percolation threshold.[29−31]

A deeper insight into the effects caused by the ϕ_{PS} value on the morphological and electrical properties of the PS NS-PEDOT:PSS films can be obtained by examining the photovoltaic performance of PSCs with PS NS-PEDOT:PSS ABL films with various ϕ_{PS} values. Figure 3 shows the $J-V$ curves of the bulk-heterojunction (BHJ) PSCs as a function of the ϕ_{PS} values under AM 1.5 illumination at 100 mW cm^{-2}. The BHJ-type PSCs were fabricated with an identical ITO/ABL/active layer/LiF/Al structure but different ϕ_{PS} values ranging from 0 to 0.9 in the PS NS-PEDOT:PSS ABL. For the active layer of the PSCs, P3HT was used as an electron donor, and OXCBA or PCBM was applied as an electron acceptor. Although the P3HT:PCBM blend is the most studied PSC

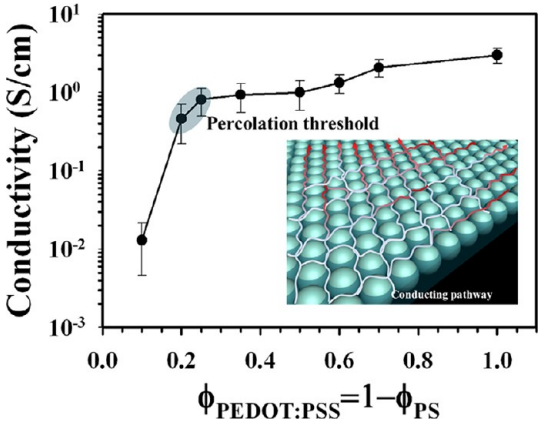

Figure 2. Conductivities of the PS NS-PEDOT:PSS films as a function of $\phi_{PEDOT:PSS}$ (= 1 − ϕ_{PS}). The scheme illustrates a conducting pathway in the PS NS-PEDOT:PSS film.

system,[39−42] because the lowest unoccupied molecular orbital (LUMO) of OXCBA is higher than that of PCBM, P3HT:OXCBA solar cells show higher V_{oc} values and greater PCE of more than 5%.[43−45] To investigate the ϕ_{PS} effects on the performance of the PSCs, the P3HT:OXCBA devices were prepared under identical conditions, including the same blend ratio of P3HT to OXCBA (1:0.6, w/w) and solvent concentration; however, the ϕ_{PS} values were different for each ABL. Thermal annealing was performed to optimize the device performance. Table 1a summarizes the device characteristics of P3HT:OXCBA BHJ PSCs with different ϕ_{PS} values. For the control ABL composed of pure PEDOT:PSS (ϕ_{PS} = 0), the device exhibited a PCE of 5.22%, an open circuit voltage (V_{OC}) of 0.85 V, a short-circuit current density (J_{SC}) of 10.30 mA cm^{-2}, and a fill factor (FF) of 0.60, which is consistent with the previously reported values.[43] As the ϕ_{PS} increased (*i.e.*, the $\phi_{PEDOT:PSS}$ decreased), the PSC performance remained greater than 5%. Notably, even at ϕ_{PS} = 0.8, the PCE of the P3HT:OXCBA device was greater than 5%, and the solar cell parameters including the V_{OC}, J_{SC}, and FF values (V_{OC}, 0.84 V; J_{SC}, 10.49 mA cm^{-2}; and FF, 0.58) were not different from that of the control sample. Finally, as ϕ_{PS} increased to 0.9, the PCE value decreased sharply to 1.05%. The observed trends in the photovoltaic performance in terms of ϕ_{PS} values were consistent with those of the conductivity and film morphology of PS NS-PEDOT:PSS films. When ϕ_{PS} is less than 0.8, PEDOT:PSS can completely fill the empty spaces between the densely packed PS NSs, creating a continuous phase that forms a conducting pathway; therefore, the PS NS-PEDOT:PSS film can successfully function as an ABL in the PSCs. In contrast, ϕ_{PS} values greater than 0.8 resulted in a volume fraction of PEDOT:PSS that was insufficient for the formation of a continuous pathway for hole conduction.[46] To further confirm the trends observed for photovoltaic performance as a function of the ϕ_{PS} value, P3HT:PCBM-based PSCs (ITO/ABL/P3HT:PCBM/LiF/Al) were fabricated using PS

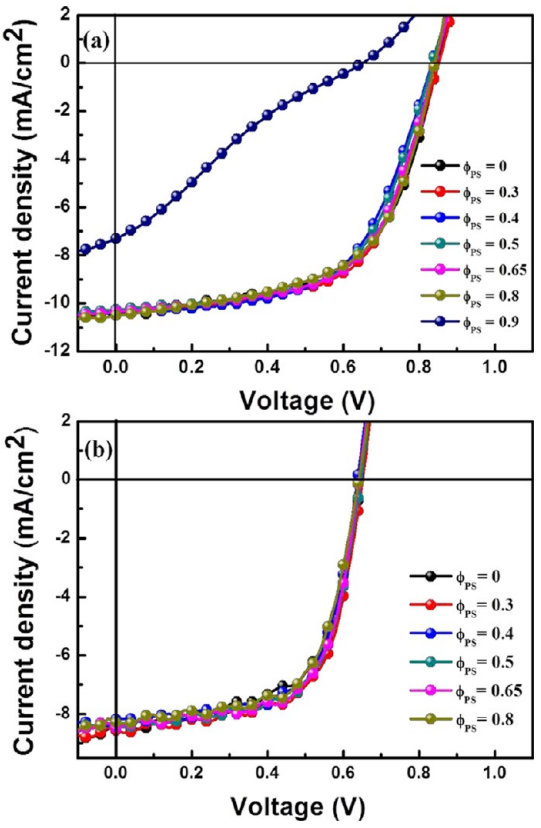

Figure 3. Current density–voltage (J–V) characteristics of PSCs with various ϕ_{PS} values for PS NS-PEDOT:PSS ABLs (ϕ_{PS} = 0, 0.3, 0.4, 0.5, 0.65, 0.8, and 0.9): (a) P3HT:OXCBA and (b) P3HT:PCBM BHJ PSCs under AM 1.5 illumination at 100 mW cm^{-2}.

NS-PEDOT:PSSs with various ϕ_{PS} values as the ABL. Figure 3b and Table 1 b compare the device characteristics of P3HT:PCBM BHJ PSCs with PS NS-PEDOT:PSS ABLs with various ϕ_{PS} values. All of the devices with ϕ_{PS} values between 0 and 0.8 showed similar performance (PCE = 3.4%). This trend was in good agreement with that obtained for the P3HT:OXCBA system.

To gain a deeper insight into the performance of PS NS-PEDOT:PSS ABLs in the PSCs, the space charge-limited current (SCLC) hole mobility was measured for devices containing ABLs with various ϕ_{PS} values (Supporting Information, Figure S2). The devices with an ITO/ABL/P3HT:OXCBA/Au structure were fabricated, resulting in a hole-only device.[47] SCLC devices containing PS NS-PEDOT:PSS ABLs with ϕ_{PS} values ranging from 0 to 0.8 had similar hole mobility values of $\sim 10^{-4}$ cm^2 V^{-1} s^{-1} (*i.e.*, at ϕ_{PS} = 0, hole mobility = 2.8 × 10^{-4} cm^2 V^{-1} s^{-1}; at ϕ_{PS} = 0.8, hole mobility = 1.4 × 10^{-4} cm^2 V^{-1} s^{-1}). All of the hole mobility values were in good agreement with the values reported for a P3HT:OXCBA device that used pure PEDOT:PSS as the ABL.[39,40,47–49] In contrast, the SCLC device with ϕ_{PS} = 0.9 had a greatly reduced hole mobility value of 8.4 × 10^{-6} cm^2 V^{-1} s^{-1}. The amount of PEDOT:PSS with ϕ_{PS} = 0.9 in the PS NS-PEDOT:PSS film was insufficient for the formation of a continuous network of PEDOT phase within the film, which resulted in lower SCLC hole mobility and hole-injection ability in the ABL and a decrease in the performance of the PSCs. And, the observed trend for the SCLC mobility was consistent with the trends observed for the electrical conductivity and PSC performance.

TABLE 1. Device characteristics of (a) P3HT:OXCBA- and (b) P3HT:PCBM-based BHJ-type PSCs using PEDOT:PSS and PS NS-PEDOT:PSS with various ϕ_{PS} values as the ABL under AM1.5 G-simulated solar illumination (100 mW cm^{-2})

active layer	ϕ_{PS}	V_{OC}	J_{SC}	FF	PCE (%)
		(a)			
P3HT:OXCBA	0	0.85	10.30	0.60	5.22
P3HT:OXCBA	0.3	0.85	10.36	0.60	5.30
P3HT:OXCBA	0.4	0.83	10.44	0.58	5.06
P3HT:OXCBA	0.5	0.84	10.27	0.60	5.12
P3HT:OXCBA	0.65	0.84	10.32	0.60	5.19
P3HT:OXCBA	0.8	0.84	10.49	0.58	5.12
P3HT:OXCBA	0.9	0.65	7.31	0.22	1.05
		(b)			
P3HT:PCBM	0	0.65	8.42	0.61	3.35
P3HT:PCBM	0.3	0.65	8.56	0.63	3.52
P3HT:PCBM	0.4	0.64	8.18	0.66	3.46
P3HT:PCBM	0.5	0.65	8.40	0.64	3.48
P3HT:PCBM	0.65	0.64	8.48	0.64	3.46
P3HT:PCBM	0.8	0.64	8.29	0.63	3.35

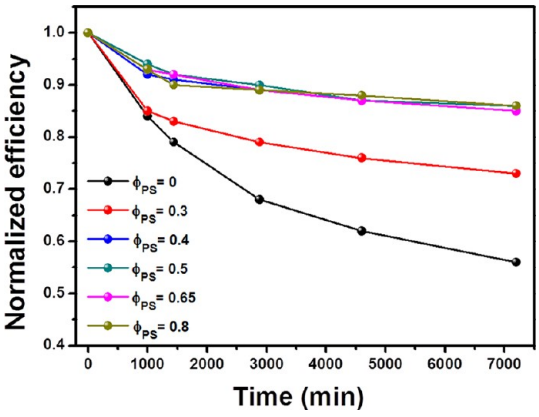

Figure 4. Air stability tests of P3HT:OXCBA PSCs with various ϕ_{PS} values in the ABL under ambient conditions.

Although the air stability of PSCs is of great importance for commercialization, the acidity and hygroscopic nature of PEDOT:PSS can negatively affect the stability of organic electronics.[15,16] Therefore, the effects of the ϕ_{PS} value on the stability of P3HT:OXCBA devices were investigated because each PS NS-PEDOT:PSS ABL film contained a different amount of PEDOT:PSS. To compare the stabilities of PSC devices with different ϕ_{PS} values, variations in device performance were measured as a function of the storage time under ambient conditions, as shown in Figure 4. The unencapsulated devices were exposed to an atmosphere of air for over 7000 min at room temperature. A clear

trend can be observed in Figure 4, which shows an enhancement in the air stability of the PSCs as the ϕ_{PS} values increased. For example, the PCE of the control device ($\phi_{PS} = 0$) decayed by ~45% after being exposed to air for 7000 min without encapsulation. In contrast, the PSC with PS NS-PEDOT:PSS ($\phi_{PS} = 0.8$) exhibited much greater air stability and 86% of the initial PCE was retained under the same measurement conditions. The improved stability was attributed mainly to the PS NSs, which reduced the degradation of the photoactive and ITO layers by the acidic conditions and the hygroscopic nature caused by the PEDOT:PSS. In addition, it is expected that, after proper surfactants are introduced into the ABL, lower volume fractions ($\phi_{PEDOT:PSS} < 0.26$) of PEDOT:PSS for the percolation threshold of the continuous conducting domain and further improvement in the stability of the PSCs can be achieved.[30,31,50−52]

CONCLUSIONS

We have successfully developed a simple and efficient method for the fabrication of semiconducting polymer blend thin films that combined the properties of electrical conductivity and enhanced stability. PS NS-PEDOT:PSS films were designed and produced by forcing the conducting PEDOT:PSS polymers into a three-dimensionally continuous minor phase *via* the self-assembly of a monolayer of 60-nm PS NSs. The resultant films were successfully applied as efficient and stable ABLs in PSCs. The effects of the addition of PS NSs with various ϕ_{PS} values on the properties of the PS NS-PEDOT:PSS layer were investigated, including the conductivity and morphological behavior. The conductivity of the PS NS-PEDOT:PSS film and the continuity of the PEDOT:PSS phase in the film were maintained, even at a low $\phi_{PEDOT:PSS}$ of 0.2−0.25. This number was in good agreement with the void space fraction between hexagonally close packed spheres, which indicated that a continuous PEDOT:PSS film was successfully formed using the PS NS template. The trend of the photovoltaic performance in terms of the ϕ_{PS} values was consistent with those of the conductivity and film morphology of the PS NS-PEDOT:PSS films. P3HT:OXCBA devices with a PS NS-PEDOT:PSS as the ABL ($\phi_{PS} = 0.8$) exhibited PCEs of over 5% with dramatically enhanced air stability. Therefore, this approach is a promising route for the production of semiconducting polymer blends with high conductivity and stability and low cost.

METHODS

Materials. Commercial PEDOT:PSS in water (PH 500, BASF), P3HT (P200, BASF) and PCBM (Nano-C) were used without further purification. The *o*-xylenyl C_{60} bis-adduct (OXCBA) was synthesized and purified as described in our previous work.[43]

Synthesis of the PS NSs. PS NSs were synthesized *via* an emulsion polymerization using a modified procedure reported previously.[53,54] Styrene monomer was purified with an aluminum oxide column. The other organic reagents were used without further purification, which included poly(vinylpyrrolidone) (PVP) (M_w = 55 000 g/mol), and 2,2-azobis-(isobutyronitrile) (AIBN). The PVP and styrene monomer were dissolved in deionized water in a 500-mL, three-neck flask and the mixture was stirred at 40 °C. After 30 min of stirring, AIBN was added to the solution. The reaction temperature was gradually increased to 70 °C. After being heated for 24 h at 70 °C, the mixture was cooled to room temperature. The resultant PS NSs were filtered and repeatedly washed by being centrifuged in deionized water to remove the residual styrene and PVP. The samples were dried in a vacuum oven at 50 °C for 12 h. The size and size distribution of the PS NSs were measured using a Hitachi S-4800 scanning electron microscope.

Sample Preparation and Conductivity Measurements. Solutions of PS NSs and PEDOT:PSS blends with different ϕ_{PS} values were prepared by mixing aqueous solutions of PS NSs and PEDOT:PSS with various ratios. The volume fraction of polymers (PS NSs + PEDOT:PSS) in the solution was controlled to produce approximately 60-nm-thick films after the solutions were spin coated onto clean glass substrate. Each solution was sonicated for 30 min at 25 °C prior to being spin coated. The films were annealed at 150 °C for 20 min to remove water. To assess the conductivity, two parallel electrodes of carbon paste were applied to the films using an adhesive mask. The measurements were performed using a two probe method at room temperature, and the voltage was supplied by a Keithley 2400 Source Meter, which ranged from −10 to 10 V across the sample. The conductivity calculations accounted for the geometry of the samples (11 mm long and 2 mm wide).

Device Fabrication and Measurements. To investigate the properties of the newly designed ABLs that consisted of PS NSs and PEDOT:PSS, BHJ photovoltaic cells using an ITO/ABL/P3HT:electron acceptor/LiF/Al structure were fabricated. The P3HT was used as an electron donor, while the PCBM and OXCBA were used as electron acceptors. The ITO-coated glass substrates were subjected to ultrasonication in acetone followed by 2% Helmanex soap in water. After the substrates were rinsed extensively with deionized water, they were ultrasonicated in deionized water followed by isopropyl alcohol. Subsequently, the substrates were dried for several hours in an oven at 80 °C. Aqueous solutions of PS NSs and PEDOT:PSS blends were prepared with various ϕ_{PS} values that ranged from 0 to 0.9. Each solution was spin coated onto a clean ITO substrate to produce approximately 60 nm-thick films. The films were annealed at 150 °C for 20 min to remove water. After the PS NS-PEDOT:PSS layer was applied, all of the subsequent procedures were performed in a glovebox under an N_2 atmosphere. Solutions of P3HT, PCBM, and OXCBA were prepared in *o*-dichlorobenzene and stirred at 100 °C overnight to ensure complete dissolution of the materials. Immediately prior to deposition, the solutions were passed through a 0.2-μm polytetrafluoroethylene syringe filter. For the P3HT:OXCBA and P3HT:PCBM devices, the solutions of P3HT:OXCBA (1:0.6 w/w) and P3HT:PCBM (1:0.7 w/w) blends were stirred at room temperature for 1 h, and then spin coated onto the ITO/PS NS-PEDOT:PSS ABL substrates at 900 rpm. The spincoating step of the P3HT/acceptor film was conducted immediately after casting the P3HT/acceptor solution in *o*-dichlorobenzene onto the ITO/PS NS-PEDOT:PSS ABL substrate. The surfactants (PVP) stabilized the PS NSs during short-term exposures to *o*-dichlorobenzene at the device-fabrication conditions (Supporting Information, Figure S3). The P3HT/acceptor film was dried and the thicknesses of films were determined to be approximately ~100 nm. Then, the substrates were placed in an evaporation chamber and held under high vacuum (*i.e.*, less than 10^{-6} Torr) for more than 1 h before a layer of LiF (approximately 0.7 nm) and Al (100 nm) were deposited on the substrate. The configuration of the shadow mask afforded four independent devices on each substrate. After the devices were fabricated, thermal annealing was performed for 5 min at 150 °C to optimize the

morphology of the BHJ active layer and improve the device performance by promoting polymer self-organization.

FE-SEM and TEM studies were performed to observe the morphology of the ABL samples using a Hitachi S-4800 and a JEOL 2000FX, respectively. The photovoltaic performances of the devices were characterized using a solar simulator (Newport Oriel Solar Simulators) with air mass 1.5 G filters. The intensity of the solar simulator was carefully calibrated using an AIST-certified silicon photodiode. The current–voltage behavior was measured using a Keithley 2400 SMU. The active area of the fabricated devices was 0.10 cm^2.

Conflict of Interest: The authors declare no competing financial interest.

Acknowledgment. This research was supported by the Korea Research Foundation Grant, funded by the Korean Government (2011-0017943).

Supporting Information Available: Additional SEM/AFM images and SCLC mobility curves. This material is available free of charge *via* the Internet at http://pubs.acs.org.

REFERENCES AND NOTES

1. Thompson, B. C.; Fréchet, J. M. J. Polymer–Fullerene Composite Solar Cells. *Angew. Chem., Int. Ed.* **2008**, *47*, 58–77.
2. Zhu, W.; Mo, Y.; Yuan, M.; Yang, W.; Cao, Y. Highly Efficient Electrophosphorescent Devices Based on Conjugated Polymers Doped with Iridium Complexes. *Appl. Phys. Lett.* **2002**, *80*, 2045–2047.
3. Sary, N.; Richard, F.; Brochon, C.; Leclerc, N.; Lévêque, P.; Audinot, J.-N.; Berson, S.; Heiser, T.; Hadziioannou, G.; Mezzenga, R. A New Supramolecular Route for Using Rod-Coil Block Copolymers in Photovoltaic Applications. *Adv. Mater.* **2010**, *22*, 763–768.
4. Arias, A. C.; MacKenzie, J. D.; McCulloch, I.; Rivnay, J.; Salleo, A. Materials and Applications for Large Area Electronics: Solution-Based Approaches. *Chem. Rev.* **2010**, *110*, 3–24.
5. Ku, S. Y.; Liman, C. D.; Cochran, J. E.; Toney, M. F.; Chabinyc, M. L.; Hawker, C. J. Solution-Processed Nanostructured Benzoporphyrin with Polycarbonate Binder for Photovoltaics. *Adv. Mater.* **2011**, *23*, 2289–2289.
6. Krebs, F. C. Fabrication and Processing of Polymer Solar Cells: A Review of Printing and Coating Techniques. *Sol. Energy Mater. Sol. Cells* **2009**, *93*, 394–412.
7. Facchetti, A. π-Conjugated Polymers for Organic Electronics and Photovoltaic Cell Applications. *Chem. Mater.* **2010**, *23*, 733–758.
8. Cho, C.-H.; Kang, H.; Kang, T. E.; Cho, H.-H.; Yoon, S. C.; Jeon, M.-K.; Kim, B. J. Controlling Side-Chain Density of Electron Donating Polymers for Improving Their Packing Structure and Photovoltaic Performance. *Chem. Commun.* **2011**, *47*, 3577–3579.
9. Cheng, Y.-J.; Yang, S.-H.; Hsu, C.-S. Synthesis of Conjugated Polymers for Organic Solar Cell Applications. *Chem. Rev.* **2009**, *109*, 5868–5923.
10. Groenendaal, L.; Jonas, F.; Freitag, D.; Pielartzik, H.; Reynolds, J. R. Poly(3,4-ethylenedioxythiophene) and Its Derivatives: Past, Present, and Future. *Adv. Mater.* **2000**, *12*, 481–494.
11. Ha, Y. H.; Nikolov, N.; Pollack, S. K.; Mastrangelo, J.; Martin, B. D.; Shashidhar, R. Towards a Transparent, Highly Conductive Poly(3,4-ethylenedioxythiophene). *Adv. Funct. Mater.* **2004**, *14*, 615–622.
12. Zhang, F. L.; Gadisa, A.; Inganas, O.; Svensson, M.; Andersson, M. R. Influence of Buffer Layers on the Performance of Polymer Solar Cells. *Appl. Phys. Lett.* **2004**, *84*, 3906–3908.
13. Carter, S. A.; Angelopoulos, M.; Karg, S.; Brock, P. J.; Scott, J. C. Polymeric Anodes for Improved Polymer Light-Emitting Diode Performance. *Appl. Phys. Lett.* **1997**, *70*, 2067–2069.
14. Snaith, H. J.; Kenrick, H.; Chiesa, M.; Friend, R. H. Morphological and Electronic Consequences of Modifications to the Polymer Anode `PEDOT:PSS'. *Polymer* **2005**, *46*, 2573–2578.
15. de Jong, M. P.; van Ijzendoorn, L. J.; de Voigt, M. J. A. Stability of the Interface between Indium-Tin-Oxide and Poly(3,4-ethylenedioxythiophene)/Poly(styrenesulfonate) in Polymer Light-Emitting Diodes. *Appl. Phys. Lett.* **2000**, *77*, 2255–2257.
16. Reese, M. O.; Morfa, A. J.; White, M. S.; Kopidakis, N.; Shaheen, S. E.; Rumbles, G.; Ginley, D. S. Pathways for the Degradation of Organic Photovoltaic P3HT:PCBM Based Devices. *Sol. Energy Mater. Sol. Cells* **2008**, *92*, 746–752.
17. Watanabe, A.; Kasuya, A. Effect of Atmospheres on the Open-Circuit Photovoltage of Nanoporous TiO_2/Poly-(3-hexylthiophene) Heterojunction Solar Cell. *Thin Solid Films* **2005**, *483*, 358–366.
18. Şahin, Y.; Alem, S.; de Bettignies, R.; Nunzi, J.-M. Development of Air Stable Polymer Solar Cells Using an Inverted Gold on Top Anode Structure. *Thin Solid Films* **2005**, *476*, 340–343.
19. Nakayama, Y.; Morii, K.; Suzuki, Y.; Machida, H.; Kera, S.; Ueno, N.; Kitagawa, H.; Noguchi, Y.; Ishii, H. Origins of Improved Hole-Injection Efficiency by the Deposition of MoO_3 on the Polymeric Semiconductor Poly-(dioctylfluorene-alt-benzothiadiazole). *Adv. Funct. Mater.* **2009**, *19*, 3746–3752.
20. Hains, A. W.; Liu, J.; Martinson, A. B. F.; Irwin, M. D.; Marks, T. J. Anode Interfacial Tuning *via* Electron-Blocking/Hole-Transport Layers and Indium Tin Oxide Surface Treatment in Bulk-Heterojunction Organic Photovoltaic Cells. *Adv. Funct. Mater.* **2010**, *20*, 595–606.
21. Lu, G.; Tang, H.; Huan, Y.; Li, S.; Li, L.; Wang, Y.; Yang, X. Enhanced Charge Transportation in Semiconducting Polymer/Insulating Polymer Composites: The Role of an Interpenetrating Bulk Interface. *Adv. Funct. Mater.* **2010**, *20*, 1714–1720.
22. Kumar, A.; Baklar, M. A.; Scott, K.; Kreouzis, T.; Stingelin-Stutzmann, N. Efficient, Stable Bulk Charge Transport in Crystalline/Crystalline Semiconductor–Insulator Blends. *Adv. Mater.* **2009**, *21*, 4447–4451.
23. Hansen, T. S.; West, K.; Hassager, O.; Larsen, N. B. Highly Stretchable and Conductive Polymer Material Made from Poly(3,4-ethylenedioxythiophene) and Polyurethane Elastomers. *Adv. Funct. Mater.* **2007**, *17*, 3069–3073.
24. Wang, H. L.; Fernandez, J. E. Conducting Polymer Blends: Polypyrrole and Poly(vinyl methyl ketone). *Macromolecules* **1992**, *25*, 6179–6184.
25. Qiu, L.; Lee, W. H.; Wang, X.; Kim, J. S.; Lim, J. A.; Kwak, D.; Lee, S.; Cho, K. Organic Thin-Film Transistors Based on Polythiophene Nanowires Embedded in Insulating Polymer. *Adv. Mater.* **2009**, *21*, 1349–1353.
26. Kietzke, T.; Neher, D.; Landfester, K.; Montenegro, R.; Guntner, R.; Scherf, U. Novel Approaches to Polymer Blends Based on Polymer Nanoparticles. *Nat. Mater.* **2003**, *2*, 408–412.
27. Macosko, C. W.; Guégan, P.; Khandpur, A. K.; Nakayama, A.; Marechal, P.; Inoue, T. Compatibilizers for Melt Blending: Premade Block Copolymers. *Macromolecules* **1996**, *29*, 5590–5598.
28. Kwon, T.; Kim, T.; Ali, F. b.; Kang, D. J.; Yoo, M.; Bang, J.; Lee, W.; Kim, B. J. Size-Controlled Polymer-Coated Nanoparticles as Efficient Compatibilizers for Polymer Blends. *Macromolecules* **2011**, *44*, 9852–9862.
29. Mezzenga, R.; Ruokolainen, J.; Fredrickson, G. H.; Kramer, E. J.; Moses, D.; Heeger, A. J.; Ikkala, O. Templating Organic Semiconductors *via* Self-Assembly of Polymer Colloids. *Science* **2003**, *299*, 1872–1874.
30. Mezzenga, R.; Ruokolainen, J.; Fredrickson, G. H.; Kramer, E. J. High Internal Phase Polymeric Emulsions by Self-Assembly of Colloidal Systems. *Macromolecules* **2003**, *36*, 4466–4471.
31. Kang, D. J.; Kwon, T.; Kim, M. P.; Cho, C.-H.; Jung, H.; Bang, J.; Kim, B. J. Creating Opal-Templated Continuous Conducting Polymer Films with Ultralow Percolation Thresholds Using Thermally Stable Nanoparticles. *Acs Nano* **2011**, *5*, 9017–9027.
32. Colard, C. A. L.; Cave, R. A.; Grossiord, N.; Covington, J. A.; Bon, S. A. F. Conducting Nanocomposite Polymer Foams

from Ice-Crystal-Templated Assembly of Mixtures of Colloids. *Adv. Mater.* **2009**, *21*, 2894–2898.
33. Bartlett, P. N.; Birkin, P. R.; Ghanem, M. A.; Toh, C.-S. Electrochemical Syntheses of Highly Ordered Macroporous Conducting Polymers Grown around Self-Assembled Colloidal Templates. *J. Mater. Chem.* **2001**, *11*, 849–853.
34. Wang, D.; Caruso, F. Fabrication of Polyaniline Inverse Opals *via* Templating Ordered Colloidal Assemblies. *Adv. Mater.* **2001**, *13*, 350–354.
35. Cassagneau, T.; Caruso, F. Semiconducting Polymer Inverse Opals Prepared by Electropolymerization. *Adv. Mater.* **2002**, *14*, 34–38.
36. Friedel, B.; Keivanidis, P. E.; Brenner, T. J. K.; Abrusci, A.; McNeill, C. R.; Friend, R. H.; Greenham, N. C. Effects of Layer Thickness and Annealing of PEDOT:PSS Layers in Organic Photodetectors. *Macromolecules* **2009**, *42*, 6741–6747.
37. Kim, Y. H.; Sachse, C.; Machala, M. L.; May, C.; Müller-Meskamp, L.; Leo, K. Highly Conductive PEDOT:PSS Electrode with Optimized Solvent and Thermal Post-treatment for ITO-Free Organic Solar Cells. *Adv. Funct. Mater.* **2011**, *21*, 1076–1081.
38. Rutgers, M. A.; Dunsmuir, J. H.; Xue, J. Z.; Russel, W. B.; Chaikin, P. M. Measurement of the Hard-Sphere Equation of State Using Screened Charged Polystyrene Colloids. *Phys. Rev. B* **1996**, *53*, 5043–5046.
39. Woo, C. H.; Thompson, B. C.; Kim, B. J.; Toney, M. F.; Fréchet, J. M. J. The Influence of Poly(3-hexylthiophene) Regioregularity on Fullerene-Composite Solar Cell Performance. *J. Am. Chem. Soc.* **2008**, *130*, 16324–16329.
40. Kim, H. J.; Han, A. R.; Cho, C.-H.; Kang, H.; Cho, H.-H.; Lee, M. Y.; Fréchet, J. M. J.; Oh, J. H.; Kim, B. J. Solvent-Resistant Organic Transistors and Thermally Stable Organic Photovoltaics Based on Cross-Linkable Conjugated Polymers. *Chem. Mater.* **2011**, *24*, 215–221.
41. Li, G.; Shrotriya, V.; Huang, J.; Yao, Y.; Moriarty, T.; Emery, K.; Yang, Y. High-Efficiency Solution Processable Polymer Photovoltaic Cells by Self-Organization of Polymer Blends. *Nat. Mater.* **2005**, *4*, 864–868.
42. Ma, W.; Yang, C.; Gong, X.; Lee, K.; Heeger, A. J. Thermally Stable, Efficient Polymer Solar Cells with Nanoscale Control of the Interpenetrating Network Morphology. *Adv. Funct. Mater.* **2005**, *15*, 1617–1622.
43. Kim, K.-H.; Kang, H.; Nam, S. Y.; Jung, J.; Kim, P. S.; Cho, C.-H.; Lee, C.; Yoon, S. C.; Kim, B. J. Facile Synthesis of *o*-Xylenyl Fullerene Multiadducts for High Open Circuit Voltage and Efficient Polymer Solar Cells. *Chem. Mater.* **2011**, *23*, 5090–5095.
44. Kim, K.-H.; Kang, H.; Kim, H. J.; Kim, P. S.; Yoon, S. C.; Kim, B. J. Effects of Solubilizing Group Modification in Fullerene Bis-Adducts on Normal and Inverted Type Polymer Solar Cells. *Chem. Mater.* **2012**, *24*, 2373–2381.
45. Voroshazi, E.; Vasseur, K.; Aernouts, T.; Heremans, P.; Baumann, A.; Deibel, C.; Xue, X.; Herring, A. J.; Athans, A. J.; Lada, T. A.; *et al*. Novel bis-C60 Derivative Compared to Other Fullerene bis-Adducts in High Efficiency Polymer Photovoltaic Cells. *J. Mater. Chem.* **2011**, *21*, 17345–17352.
46. Sangeeth, C. S. S.; Manu, J.; Reghu, M. Correlation of Morphology and Charge Transport in Poly(3,4-ethylenedioxythiophene)–Polystyrenesulfonic Acid (PEDOT–PSS) Films. *J. Phys.: Condens. Matter.* **2009**, *21*, 072101.
47. Mihailetchi, V. D.; Xie, H. X.; de Boer, B.; Koster, L. J. A.; Blom, P. W. M. Charge Transport and Photocurrent Generation in Poly(3-hexylthiophene): Methanofullerene Bulk-Heterojunction Solar Cells. *Adv. Funct. Mater.* **2006**, *16*, 699–708.
48. Kang, H.; Cho, C.-H.; Cho, H.-H.; Kang, T. E.; Kim, H. J.; Kim, K.-H.; Yoon, S. C.; Kim, B. J. Controlling Number of Indene Solubilizing Groups in Multiadduct Fullerenes for Tuning Optoelectronic Properties and Open-Circuit Voltage in Organic Solar Cells. *ACS Appl. Mater. Interfaces* **2011**, *4*, 110–116.
49. Dante, M.; Peet, J.; Nguyen, T.-Q. Nanoscale Charge Transport and Internal Structure of Bulk Heterojunction Conjugated Polymer/Fullerene Solar Cells by Scanning Probe Microscopy. *J. Phys. Chem. C* **2008**, *112*, 7241–7249.
50. Li, Z.; Ming, T.; Wang, J.; Ngai, T. High Internal Phase Emulsions Stabilized Solely by Microgel Particles. *Angew. Chem., Int. Ed.* **2009**, *48*, 8490–8493.
51. Kim, B. J.; Fredrickson, G. H.; Bang, J.; Hawker, C. J.; Kramer, E. J. Tailoring Core–Shell Polymer-Coated Nanoparticles as Block Copolymer Surfactants. *Macromolecules* **2009**, *42*, 6193–6201.
52. Cameron, N. R. High Internal Phase Emulsion Templating as a Route to Well-Defined Porous Polymers. *Polymer* **2005**, *46*, 1439–1449.
53. Bamnolker, H.; Margel, S. Dispersion Polymerization of Styrene in Polar Solvents: Effect of Reaction Parameters on Microsphere Surface Composition and Surface Properties, Size and Size Distribution, and Molecular Weight. *J. Polym. Sci., Part A: Polym. Chem.* **1996**, *34*, 1857–1871.
54. Du, X.; He, J. Facile Size-Controllable Syntheses of Highly Monodisperse Polystyrene Nano- and Macrospheres by Polyvinylpyrrolidone-Mediated Emulsifier-free Emulsion Polymerization. *J. Appl. Polym. Sci.* **2008**, *108*, 1755–1760.